Hindawi
Geofluids
Volume 2019, Article ID 1672418, 14 pages
https://doi.org/10.1155/2019/1672418

Research Article

A New Soil-Water Characteristic Curve Model for Unsaturated Loess Based on Wetting-Induced Pore Deformation

Yuwei Zhang[1,2] **Zhanping Song**[1,2] **Xiaolin Weng**[3] **and Yongli Xie**[3]

[1]*School of Civil Engineering, Xi'an University of Architecture and Technology, Xi'an 710055, China*
[2]*Shaanxi Key Laboratory of Geotechnical and Underground Space, Xi'an University of Architecture and Technology, Xi'an 710055, China*
[3]*School of Highway, Chang'an University, Xi'an 710064, China*

Correspondence should be addressed to Yuwei Zhang; 1032659676@qq.com and Zhanping Song; songzhpyt@xauat.edu.cn

Received 27 November 2018; Revised 24 January 2019; Accepted 20 February 2019; Published 15 April 2019

Academic Editor: Jaewon Jang

The soil-water characteristic curve (SWCC) is the basis for describing seepage, strength, and constitutive model of unsaturated soil. The existing SWCC models do not work accurately for evaluating loess, because they do not consider the pore deformation that is induced by wetting. The present study develops a new SWCC model for unsaturated loess. The model considers the effect of wetting-induced pore deformation (WIPD) on the SWCC. The new model includes 6 parameters, which could be confirmed by laboratory tests. The pore volume function (PVF) was described by the WIPD. The shift factor ξ_{1i} and the compression factor ξ_{2i} were introduced into the model. The relationship between the void ratio e and ξ_{1i} and ξ_{2i} was established using the average pore radius. The new SWCC model for saturated loess was improved based on the classical van Genuchten (V-G) model. If the WIPD had not been considered, the new model would regress into the classical V-G model. SWCC tests of unsaturated loess with different void ratios were carried out to verify the new model. The model parameters were calibrated in the original state, and the SWCCs of different void ratios were predicted by the new model and found to be in good agreement with the test results.

1. Introduction

Loess covers a considerable part of China, especially in northern China's Loess Plateau, where thick, unsaturated, and collapsible loess abounds. The properties of unsaturated loess are sensitive to water content [1]. The inner pores of this material are obviously influenced by wetting. Wetting-induced pore deformation (WIPD) is the main reason for changes in the hydraulic characteristics of loess [2–5]. The loess material used in construction work is mostly in an unsaturated state. The unique solid-liquid-gas state of unsaturated loess complicates its mechanical properties. The soil-water characteristic curve (SWCC) is the basis of the study of loess mechanics, which is a field of study that describes the relationship between saturation (S_r) or volumetric moisture content (θ) and suction (s). The hydromechanical properties of unsaturated soil, such as permeability [6, 7], strength [8–12], and deformation [13–19], are closely related to the SWCC. The constitutive model often involves the SWCC [20–28]; therefore, some scholars have pointed out that the SWCC has the same status in unsaturated soil mechanics as the compression curve has in saturated soil mechanics [29–33]. Measurement of the SWCC by laboratory and field methods is time-consuming and expensive; therefore, it is helpful to establish a mathematical SWCC model for predicting the hydraulic characteristics of soil [34–36].

Much research has been conducted on the theoretical model of the SWCC. According to some studies, the SWCC is influenced by multiple factors, including temperature [37], drying and watering cycles [38–40], stress history [41, 42], and initial density [43–45], in which the pore structure of the soil has a decisive influence on the SWCC [46–49]. Early SWCC models used the pore distribution coefficient to reflect the influence of the pore structure. In these models, the pore structure was usually assumed to consist of rigid pores that were unaffected by deformation [50–53]. This assumption is applicable to conventional soils. However, if pore deformation is not considered in the case of highly

collapsible and unsaturated loess with large pores, the predictions will have significant errors.

In follow-up studies, scholars have gradually realized this limitation [54–56], and they have begun to explore the SWCC model with consideration of the influence of pore change. Researchers have conducted tests to obtain the SWCC with different void ratios, and some have established empirical models based on test results. For example, Sun et al. [57, 58] conducted an SWCC test of red clay, analyzing the variation law of the SWCC and the characteristics of wetting-drying hysteresis for different types of pores. Rahardjo et al. [59] carried out a complete dehumidification test of expansive soil, analyzing changes in the SWCC of different initial void ratios; Zhou et al. [45] analyzed the incremental relationship between saturation and initial density, introducing an initial density influence factor to build an SWCC model. Simms and Yanful gauged the variation pattern of pores in a clay dehumidification test, establishing a causality relationship between pore distribution and the SWCC [60]. Zhang and Chen [61] introduced the average pore, pore distribution index, and porosity, combining these factors with the Brooks and Corey model to construct an SWCC model for deformed soil. Other scholars introduced a variety of parameters (void ratio, dry density, etc.) into the existing classical model through a series of assumptions, to reflect the influence of the pore change on the SWCC. For instance, considering the influence of the void ratio on parameters such as the suction intake value and pore distribution index, Huang et al. [7] established an SWCC model based on the Brooks and Corey model. Gallipoli [31] defined the relationship between the parameters of the suction intake value and the void ratio and established an SWCC model. Nuth and Laloui [62] defined the influence pattern of soil compression deformation on soil pores and established a cooperative relationship between soil compression and the SWCC. Hu et al. [49] assumed that pore functions remain unchanged during compression deformation and established an SWCC model that considered deformation. Scholars have carried out much research on soil-water characteristics using experimental tests [39, 57, 58], theories [2, 3, 8, 10, 28, 31], and numerical modeling methods [63, 64]; however, studies on the impact of wetting-induced pore deformation (WIPD) on the SWCC of unsaturated loess are limited.

Previous research has shown that the size distribution of soil pores evolves with changes in the hydraulic path and stress history [2, 18, 39, 47]. The description of a pore distribution index has involved different analytical methods in different models. A reasonable pore evolution law can simulate the evolution of aggregate pore structures and the hydraulic changes of compact loess [47, 49, 52, 54, 65]. In this paper, the authors took the pore volume function (PVF) as the basis, considered the evolutionary characteristics of immersed pore structures, and assumed the influence law of WIPD on the PVF. The compression factor and the shift factor were introduced into PVF under the impact of WIPD. Based on the classical V-G model [66], a new SWCC model of loess that considers the effect of WIPD was established in this paper. There are six parameters (θ_s, θ_r, m, a, e_0, and b) in the new model, all of which could be calibrated by simple laboratory tests. Finally, results from the SWCC tests of the reconstructed unsaturated loess with different void ratios are used to verify the capability of the new model. The influence of each parameter on the new model was discussed in detail. The research results of this paper can provide a new simplified and accurate method for predicting the SWCC of loess resulting from WIPD.

2. Evolution Characteristics of WIPD in Loess

2.1. Pore Distribution Function. Unsaturated loess could be taken as a porous medium composed of pores and particles with different sizes. The radius of the pores is r, and the PVF of the porous medium is $f(r)$. So when the radius of the pores changes from r to $r + dr$ and the percentage taken up of the pores is $f(r)dr$, the pore volume in the soil can be expressed as

$$\int_0^{\infty} f(r)dr. \tag{1}$$

Given the assumption that the radius of all pores in the loess falls in the range between the minimum radius $r_{\min}$ and the maximum radius $r_{\max}$ and according to the definition of volumetric moisture content and the assumption of local equilibrium, pores with a radius that is smaller than that of a certain value R will be filled by water. Therefore, the relationship between the volumetric moisture content and the PVF can be expressed as follows

$$\theta(s) = \int_{r_{\min}}^{R} f(r)dr. \tag{2}$$

When the definition of the soil water-holing capacity curve (capillary pressure distribution function) is taken into consideration [20],

$$g(s) = \frac{d\theta}{ds} = \frac{f(r)dr}{ds}. \tag{3}$$

The study of Zhou et al. [22, 44] holds that water in soil pores may be classified into two categories, one being the free water inside the pores with significant capillarity and the other being the water that is attached to solid particles. By means of the impact of chemical bonding, the latter kind of water is considered to be unchanged and thus equal to residual saturation S_r^{res}. It corresponds to the residual volumetric moisture content θ_r. Since the saturation of soils was regarded as the sum of microsaturation S_r^m and macrosaturation S_r^M, then $S_r = S_r^m + S_r^M$. Volumetric moisture content can also be regarded as being composed of the residual volumetric moisture content and the volumetric moisture content of the changing part. Therefore, the relationship between the volumetric moisture content and the PVF meets the following conditions:

$$\theta(s) = \int_{r_{\min}}^{R} f(r)dr + \theta_r. \tag{4}$$

The water-holding capacity curve function in equation (3) is expressed in the following way:

$$\theta(s) = \int_{+\infty}^{s} g(s)ds + \theta_r. \tag{5}$$

When the soil suction is infinite ($s \to +\infty$), the volumetric moisture content of soils is the residual volumetric moisture content ($\theta(s) = \theta_r$), and the soil saturation is the residual saturation ($S_r = S_r^m = S_r^{\text{res}}$). When the soil suction is zero ($s = 0$), the volumetric moisture content is $\theta(s) = \int_{+\infty}^{0} g(s)ds + \theta_r$, and the saturation is 1, $S_r = S_r^s = 1$.

Effective saturation is defined as [22]

$$S_e = \frac{\theta - \theta_r}{\theta_s - \theta_r} \tag{6}$$

and is expressed using the PVF thusly

$$S_e = \frac{\int_{R_{\min}}^{R} f(x)dx}{\int_{R_{\min}}^{R_{\max}} f(x)dx}. \tag{7}$$

And it is expressed using the water-holding capacity curve function thusly

$$S_e = \frac{\int_{+\infty}^{s} g(x)dx}{\int_{+\infty}^{0} g(x)dx}. \tag{8}$$

Judging from equations (7) and (8), we can find that to deduce the SWCC, the PVF or the water-holding capacity curve function must be known. The PVF can be also expressed by the pore density function. In this paper, the method proposed by Della Vecchia et al. [47] is used to deduce the pore density function $\text{psd}(r)$, and $F^e(R)$ is denoted as the contribution of pores with a radius less than R to the overall void ratio. Variable $F^e(R)$ is defined as follows:

$$F^e(R) = e \cdot F(R) = e_w(R). \tag{9}$$

According to the local equilibrium assumption raised by Mualem [6], water inside soil first fills up small pores due to the higher capillarity. The pore radius integral function $F(R)$ at this time can be linked with the saturation of soils:

$$S_r(R) = F(R). \tag{10}$$

And $\text{psd}(r)$ is defined as the pore size density function of the porous medium, such that when the pore radius changes from r to $r + dr$, the percentage occupied by the pores is $\text{psd}(r)dr$. Hence,

$$\int_0^{\infty} \text{psd}(r)dr = 1. \tag{11}$$

The radius of all pores in the soil falls between the minimum radius $r_{\min}$ and the maximum radius $r_{\max}$, and thus,

$$\int_{r_{\min}}^{r_{\max}} \text{psd}(r)dr = 1. \tag{12}$$

$F(R)$ is denoted as the probability of pores with less-than R radius, and the number of pores with radius that is smaller than R is

$$F(R) = \int_{r_{\min}}^{R} \text{psd}(r)dr. \tag{13}$$

The typical diagram of pore distribution is shown in Figure 1. A specific suction s corresponds to a specific pore radius r. Pores with a radius that is larger than r in the soil are filled up by air, while those with less-than r radius are filled up by water. According to the definition of soil saturation, the relationship between saturation and pore distribution is as follows:

$$S_r(R) = F(R) = \int_{r_{\min}}^{R} \text{psd}(r)dr. \tag{14}$$

The moisture content ratio is gained by the following:

$$e_w(R) = F^e(R) = eF(R) = eS_r(R). \tag{15}$$

Based on the definition of PVF from the research of Della Vecchia et al. [47],

$$f(r) = \frac{dF^e(r)}{d(\ln(r))} = \frac{e \cdot dS_r(R)}{d(\ln(r))}. \tag{16}$$

Moreover, according to the Young-Laplace equation, the relationship between pore radius and suction is as follows:

$$s = \frac{2T\cos\alpha}{r}, \tag{17}$$

where s is the suction, T is the surface tension of pore water, α is the contact angle between pore water and particles, and r is the pore radius. For a specific soil, the mineral composition and pore liquid composition remain unchanged. Therefore, $2T\cos\alpha$ is considered the constant C.

The function of the relationship between saturation and suction satisfies the following:

$$S_r(R) = \int_{r_{\min}}^{R} \text{psd}(r)dr = \int_{r_{\min}}^{R} \text{psd}\left(\frac{2T\cos\alpha}{s}\right)dr = G(s), \tag{18}$$

where $G(s)$ represents the SWCC model. As seen, we could derive the PVF from the existing SWCC model.

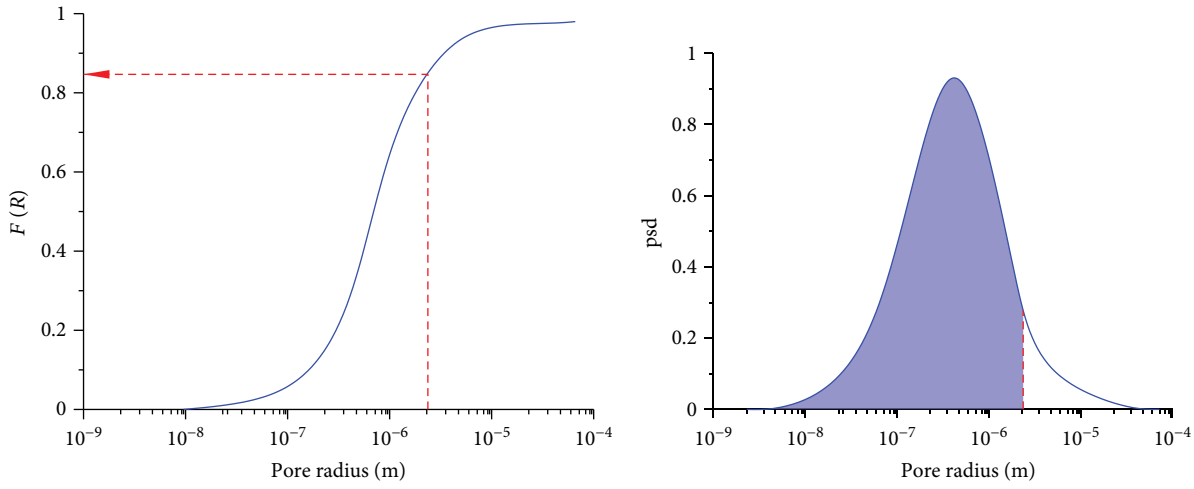

Figure 1: Typical diagram of pore distribution.

The classical V-G model was used for the derivation. The SWCC function of the V-G model is represented as [66]

$$S_r(s) = \frac{1}{(1 + (\alpha s)^n)^m}. \tag{19}$$

The derivation process involves the following: based on the definition of the volumetric moisture content, the following is obtained thusly:

$$F^e(R) = e \cdot S_r(R) = e\frac{1}{(1 + (\alpha s)^n)^m} = e\frac{1}{(1 + (\alpha C/r)^n)^m}. \tag{20}$$

The pore density function that takes volumetric moisture content into consideration is as follows:

$$\mathrm{psd}^e(R) = \frac{dF^e(R)}{dr} = \frac{\alpha C m n e}{r^2}\left[1 + \left(\frac{\alpha C}{r}\right)^n\right]^{(-m-1)}\left(\frac{\alpha C}{r}\right)^{n-1}. \tag{21}$$

The PVF is

$$f(r) = \frac{dF^e(R)}{d\ln r} = \mathrm{psd}^e(r) \cdot r = mne\left[1 + \left(\frac{\alpha C}{r}\right)^n\right]^{(-m-1)}\left(\frac{\alpha C}{r}\right)^n. \tag{22}$$

In equation (22), $f(r)$ is the expression of the PVF of the soil when the V-G model is selected.

After the PVF of the soil is obtained, the description of the influence of WIPD on the SWCC must be preceded by establishing how the PVF changes with variations in WIPD. This means that the influence of WIPD on the PVF should be determined first. In the next section, we will consider the patterns in the influence exerted by WIPD on the PVF of the loess.

2.2. Influence of WIPD on PVF. Much research has been conducted on the influence of processes like loading [25, 41], humidification [20, 40], and drying-and-watering cycles [12, 38, 39] on the pore structure of loess. These studies have made important discoveries that pores between the aggregates are sensitive to the process of loading and humidification; the pore radius decreases significantly with the increase of the consolidation pressure; the pattern of the deformation of pores between the aggregates is complex and closely related to the soil type and stress history; and the pores in the aggregates will be destroyed after the pores between the aggregates are destroyed under the influence of the disturbing action. Tanaka et al. [65] carried out mercury injection tests on soil samples compressed differently (shown in Figure 2) and studied the changes in soil pore structure under deformation conditions. Monroy et al. [52] conducted mercury injection tests and electron microscopy tests on London clay in the conditions of humidification and analyzed the microstructure evolution law. Lloret et al. [51] carried out mercury injection tests of silt under different compression saturation conditions (shown in Figure 3) and discussed the influence of compression deformation on microscopic pores. Hu et al. [49] summarized the mercury injection test results of various soil samples conducted by Tanaka et al. [65] and went on to argue that the general form of pore distribution did not undergo significantly during compression. It is further assumed that the pore distribution function can be obtained by shifting and scaling in semi-logarithmic coordinates, and that amount of shifting and scaling is related to the pore structure indicator. Considering that during the process of loess immersion, the macropores (interaggregate pores) collapse first, the micropores (intra-aggregate pores) are relatively stable, and the WIPD can be simplified into a single-peak regular change [49]. Therefore, the above concept is also used to establish the causal

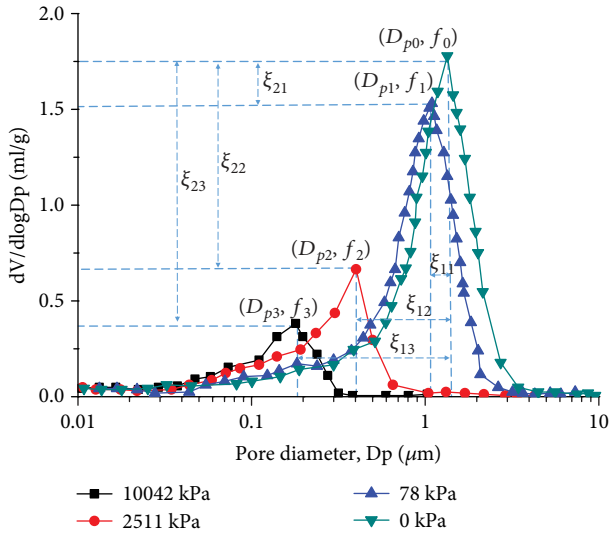

Figure 2: MIP results of dromedary soil [63].

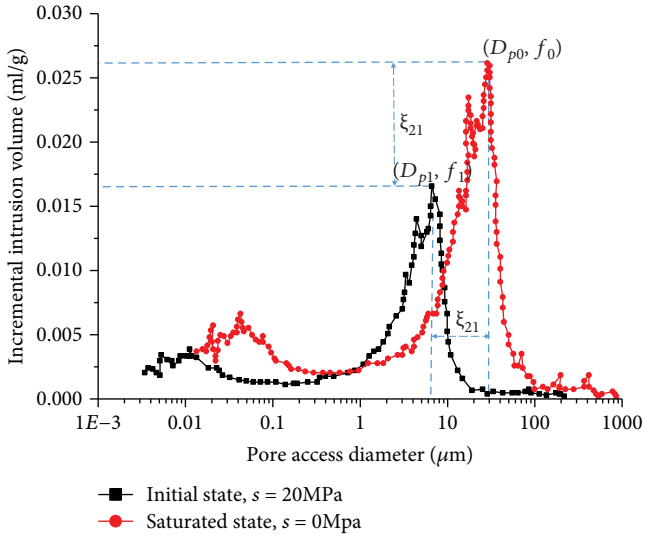

Figure 3: MIP results of bimodal soil [51].

relationship between WIPD and the PVF. Since the PVF's shape remains unchanged during the process of WIPD, the compression factor and the shift factor are introduced to characterize the influence of water immersion on the PVF.

Based on the assumed pattern of the influence of WIPD of unsaturated loess on the PVF, the soil simplification may be regarded as a dromedary structure without considering the pore variation in the aggregate. The influence of WIPD on the PVF of the loess can be obtained by shifting and scaling from an initial state. This means that the PVF of any pore deformation state can be obtained through the PVF of the initial state. By introducing the shift factor ξ_{1i} and the compression factor ξ_{2i} and by establishing the relationships of the pore indicator e and shift factor and compression factor through average pore radius, the PVF under any state of

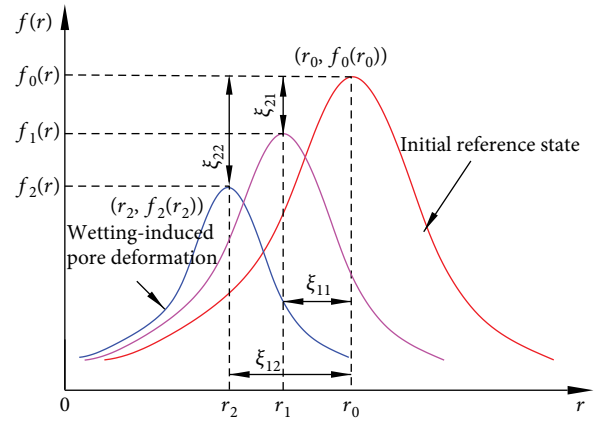

Figure 4: Influence of pore deformation on PVF.

WIPD can be expressed. As shown in Figure 4, the shift factor ξ_{1i} and the compression factor ξ_{2i} can be expressed as

$$\xi_{1i} = \frac{r_i}{r_0}, \tag{23}$$

$$\xi_{2i} = \frac{f_i(r_i)}{f_0(r_0)}. \tag{24}$$

It can be imagined that so long as the relationships between the indicator of the soil pores (such as void ratio, porosity factor, etc.) and the shift factor and the compression factor are established, the PVF of any state under different pore indicators can be obtained, based on which the SWCC under any pore deformation state can be obtained by integration from equation (7).

3. SWCC Model considering WIPD

3.1. Deduction of PVF at the Initial State. Taking the V-G model as the basis and assuming an initial state in which the void ratio of any pore is proposed as e_0, the PVF at the initial state is denoted as $f_0(r)$, and the expression of which is as follows:

$$f_0(r) = mne_0\left[1 + \left(\frac{\alpha C}{r}\right)^n\right]^{(-m-1)}\left(\frac{\alpha C}{r}\right)^n. \tag{25}$$

First, to obtain the peak value $f(r_0)$ at the initial reference state, we take the derivative of the PVF, as follows:

$$\frac{\partial f_0(r)}{\partial \ln r} = r\cdot\left[(m+1)n\cdot\left(1+\left(\frac{\alpha C}{r}\right)^n\right)^{-m-2}\cdot\left(\frac{\alpha C}{r}\right)^{n-1}\cdot\left(\frac{\alpha C}{r^2}\right)\cdot\left(\frac{\alpha C}{r}\right)^n - \left(1+\left(\frac{\alpha C}{r}\right)^n\right)^{-m-1}\cdot\left(\frac{\alpha C}{r}\right)^{n-1}\cdot\left(\frac{\alpha C}{r^2}\right)\right]. \tag{26}$$

Assume that $((\partial f_0(r))/\partial \ln r) = 0$ and r_0 can be gained through further simplification:

$$r_0 = \alpha C \sqrt[n]{m}. \tag{27}$$

Substitute r_0 into the PVF, and obtain the following:

$$f_0(r_0) = mne_0\left(1 + \frac{1}{m}\right)^{-m-1}. \tag{28}$$

In the same way, the PVF at any state can be gained as

$$f_i(r_i) = mne_i\left(1 + \frac{1}{m}\right)^{-m-1}. \tag{29}$$

3.2. Shift Factor ξ_{1i} and Compression Factor ξ_{2i}. Combining the PVF with the definition of the compression factor ξ_{2i}, we obtain

$$\xi_{2i} = \frac{f_i(r_i)}{f_0(r_0)} = \frac{mne_i(1 + (1/m))^{-m-1}}{mne_0(1 + (1/m))^{-m-1}} = \frac{e_i}{e_0}. \tag{30}$$

Then, we solve for the shift factor ξ_{1i}.

According to the definition in equation (23), the average pore radius at a certain pore state is

$$\xi_{1i} = \frac{\overline{r}_i}{\overline{r}_0}. \tag{31}$$

It can be found that to solve and obtain the shift factor ξ_{1i}, the expression of the soil average pore radius should first be obtained. The relationship between the shift factor ξ_{1i} and the pore indicator can be obtained by deduction from the average pore radius. According to the aforesaid definition of the PVF $f(r)$, we use the pore volume proportion as the weight and combine it with the PVF to obtain the expression of the average pore radius, as follows:

$$\overline{r} = \frac{\int_{r_{\min}}^{r_{\max}} rf(r)dr}{\int_{r_{\min}}^{r_{\max}} f(r)dr}. \tag{32}$$

We associate this with the Young-Laplace equation in equation (17) and substitute the volumetric moisture content to obtain the following:

$$\overline{r} = \frac{C\int_{\theta_r}^{\theta_s}(1/s)d\theta}{\int_{\theta_r}^{\theta_s} 1 d\theta}. \tag{33}$$

To simplify the derivation process, we select the B-C model with relatively few model parameters to solve $\overline{r}$. The relational expression (expressed by volumetric moisture content and suction) is as follows:

$$\theta = \theta_r + (\theta_s - \theta_r) \cdot \left(\frac{s_a}{s}\right)^{\lambda}, \quad s \geq s_a. \tag{34}$$

We convert it into

$$\frac{1}{s} = \frac{1}{s_a}\left(\frac{\theta - \theta_r}{\theta_s - \theta_r}\right)^{1/\lambda}. \tag{35}$$

We substitute this into the above equation and obtain

$$\overline{r} = \int_{\theta_r}^{\theta_s}\left[\frac{C}{s_a}\left(\frac{\theta - \theta_r}{\theta_s - \theta_r}\right)^{(\lambda+1)/\lambda}\left(\frac{\lambda}{\lambda+1}\right)\right] = \frac{C}{s_a}\left(\frac{\lambda}{\lambda+1}\right) = C \cdot r_a, \tag{36}$$

where r_a is the average pore radius indicator. We obtain the relational expression between the average pore radius and void ratio:

$$n = \left(\frac{r_a}{a + r_a}\right)^b = \left(\frac{\overline{r}_i/C}{(a + \overline{r}_i)/C}\right)^b = \frac{e}{1+e}. \tag{37}$$

Further, we obtain the average pore radius:

$$\overline{r}_i = \frac{aC(e_i/(1+e_i))^{1/b}}{1 - (e_i/(1+e_i))^{1/b}}. \tag{38}$$

We substitute it into equation (31) and obtain

$$\frac{1}{\xi_{1i}} = \frac{\overline{r_0}}{\overline{r_i}} = \frac{aC(e_0/(1+e_0))^{1/b}}{1 - (e_0/(1+e_0))^{1/b}} \cdot \frac{1 - (e_i/(1+e_i))^{1/b}}{aC(e_i/(1+e_i))^{1/b}}. \tag{39}$$

We simplify and dispose it and get:

$$\frac{1}{\xi_{1i}} = \frac{(e_0/(1+e_0))^{1/b}\left[1 - (e_i/(1+e_i))^{1/b}\right]}{\left[1 - (e_0/(1+e_0))^{1/b}\right](e_i/(1+e_i))^{1/b}}. \tag{40}$$

3.3. Model Establishing. The PVF $f_i(r)$ in any state can be found after combining the initial reference-state PVF $f_0(r)$ (obtained on the basis of the V-G model), the shift factor ξ_{1i}, and the compression factor ξ_{2i}:

$$f_i(r_i) = \xi_{2i} f_0(\xi_{1i} r_0) = \xi_{2i} mne_0\left[1 + \left(\frac{aC}{\xi_{1i} r_0}\right)^n\right]^{(-m-1)}\left(\frac{aC}{\xi_{1i} r_0}\right)^n. \tag{41}$$

The SWCC (equation (3)) of any pore state is

$$g_i(r) = \frac{f_i(r)dr}{ds}. \tag{42}$$

We introduce the SWCC of any state into the SWCC integration function (equation (8)) to obtain the SWCC at any pore state:

$$S_e = \frac{\int_{+\infty}^{s} g_i(x)dx}{\int_{+\infty}^{0} g_i(x)dx} = \frac{\int_{+\infty}^{s} (\xi_{2i} mne_i/n)\left(1 + (as/\xi_{1i})^n\right)^{-m} ds}{\int_{+\infty}^{0} (\xi_{2i} mne_i/n)\left(1 + (as/\xi_{1i})^n\right)^{-m} ds}. \tag{43}$$

We simplify this and obtain

$$S_e = \left(1 + \left(\frac{as}{\xi_{1i}}\right)^n\right)^{-m}. \tag{44}$$

We introduce ξ_{1i} (equation (40)) into equation (44) and obtain

$$S_e = \left(1 + \left(\alpha \frac{(e_0/(1+e_0))^{1/b}\left[1 - (e_i/(1+e_i))^{1/b}\right]}{\left[1 - (e_0/(1+e_0))^{1/b}\right](e_i/(1+e_i))^{1/b}} s\right)^n\right)^{-m}. \tag{45}$$

Thus, we find that the SWCC at any pore state is expressed as the function between the suction and void ratio. The SWCC changes with the void ratio changes. This can be construed as the three-dimensional space curve composed of saturation degree, suction, and void ratio. When the void ratio is not taken into consideration, we take the reference state $e_i = e_0$. At this point, the SWCC regresses into the classical V-G model. Hence, we deem that the V-G model is just a special form of the model in this paper.

4. Model Verification

4.1. SWCC Tests of Unsaturated Loess

4.1.1. Test Instrument. The SWCC test methods [35, 55] include primarily the pressure plate extractor method, salt solution method, filter paper method, Tempe instrument method, tension meter method, shaft shifting technique method, dew-point potentiometer method, and TDR matrix suction test method. The tests in this paper used the 15 bar (1 bar = 100 kPa) pressure membrane meter produced by the American Soil Moisture Instrument Company. As shown in Figure 5, the test system consists of an air booster pump, control valve, pressure chamber, and water collecting system. The air booster pump provides pressure, and the control valve controls the pressure during the test process. The pressure chamber is a cylindrical steel cylinder, which has a pressure-maintaining effect. The lower part of the chamber is a ceramic plate, sealed by kaolin roasting. Once the water is saturated, air cannot pass through the ceramic plate, due to the film shrinkage effect. When the pressure chamber reaches an equilibrium, the suction value of the soil is equal in value to the applied pressure value; that is, the suction value in any state of the soil can be directly read out by the pressure control system. The water collecting system collects the water discharged under different pressures, and it can monitor the corresponding displacement under different pressures at any time and then calculate the volumetric moisture content of the soil.

Figure 5: 15 bar pressure membrane.

The working mechanism of the pressure membrane meter is as follows: it blocks the air from entering the pressure chamber through the ceramic plate; the membrane will produce surface tension as the pores of the ceramic plate shrink; the shrunk membrane covers the small hole of the whole ceramic plate; the difference between the gas pressure above the shrunk membrane and the water pressure below it is equal to the suction value; and the maximal suction value that can be maintained by the ceramic plate is $s_d = (u_a - u_w)_d = 2T_s/R_s$. In this equation, s_d represents the ceramic plate inlet value, T_s is the surface tension caused by the shrunk membrane; and R_s is the radius of the curvature of the shrunk membrane between the pores or the maximum pore radius. The liquid phase water in the soil passes through the porous ceramic plate under pressure, and it reaches an equilibrium in the reverse pressure state. Then, the pressure boost value of the pressure control system is the suction value, and the saturation of the soil can be calculated by the amount of discharged water. The SWCC of the tested soil is obtained ultimately.

4.1.2. Test Plan and Process. In this work, we set out to conduct tests of the SWCC of loess during the loess drying process. Remolded loess samples with different void ratios were prepared in the process that took the impact of the WIPD of unsaturated loess into consideration. The samples were prepared by fully disturbing the undisturbed soil, which was directly obtained from a construction site, packaged, and transported to the laboratory. The fundamental parameters of the undisturbed soil were tested and recorded, as shown in Table 1. The void ratios of different remolded soil samples were considered to be 0.85, 0.8, 0.75, 0.7, 0.65, and 0.6, and the corresponding dry densities were 1.47 g/cm^3, 1.51 g/cm^3, 1.55 g/cm^3, 1.60 g/cm^3, 1.65 g/cm^3, and 1.70 g/cm^3, respectively. The pressure boost values during the test process were set, respectively, at 0.1 bar, 0.2 bar, 0.4 bar, 0.6 bar, 0.8 bar, 1 bar, 1.5 bar, 2 bar, 2.5 bar, 3 bar, 3.5 bar, 4 bar, 4.5 bar, and 5 bar; the corresponding suction values were, respectively, 10 kPa, 20 kPa, 40 kPa, 60 kPa, 80 kPa,

Table 1: Parameters of undisturbed loess.

Specific gravity (G_s)	Density (g/cm^3)	Water content (%)	c (kPa)	Void ratio	φ (°)	Compression modulus (MPa)
2.72	1.52	14.1	30.66	0.82	21	12.6

100 kPa, 150 kPa, 200 kPa, 250 kPa, 300 kPa, 350 kPa, 400 kPa, 450 kPa, and 500 kPa.

The remolded soil sample was prepared by fully disturbing the undisturbed soil, and the remolded samples with different void ratios were prepared using the sampler (Figure 6). The test principle for preparing the remolded soil samples of different void ratios is as follows: the small ring cutter had a volume of $V = \pi r^2 h = 59.99\ \text{cm}^3$. According to the definition of dry density $\rho_d = m_s/V$, the amount of dry soil m_s required for different dry densities ρ_d was obtained. The water content was set to be the same as that of the undisturbed soil. The amount of water used for a small ring cutter sample could then be calculated. The amount of dry soil m_s and the required amount of water were weighed, before they were thoroughly mixed and simmered for 48 hours. Two 4 cm sample-pressure blocks were placed in the pressure cylinder, and the prepared soil material was placed in the pressure cylinder. A 2 cm pressure piece was placed on top of the material, and the material was finally compressed by a 4 cm pressure piece to reach the brim of the pressure cylinder. The pressed sample was pushed out and placed in a small ring cutter to obtain the desired sample of the void ratio. Remolded loess samples with different void ratios were prepared using the method above in turn.

According to the requirements of the tests, samples were saturated by the capillary saturation method. The saturation of the ring cutter sample was measured after saturation for 72 hours. The samples were deemed to meet the requirements if the saturation was greater than 95%. We wet the ceramic plate to a saturated state before the test. We weighed and recorded the total weight of the ring cutter plus the soil and then sealed the pressure chamber and exerted pressure step by step. After each stage of pressure balance, we read and recorded the reading of the water-collecting tube and used the difference between the two balance readings to determine the drainage weight that corresponded to each stage of pressure $m_{wj} = \alpha \cdot \Delta h$, where α is the calibration parameter of the water-collecting tube with the unit being g/mm and Δh is the difference between the readings of the water-collecting tube after the two balances with the unit being mm. When the maximum pressure was applied to the soil and stabilized, we took out the ring cutter sample and weighed it and then dried and weighed it again. Thus, the moisture content weight at the maximum level of suction stability was gained and is denoted as m_{wf}. Then, the weight of the water at each level of suction was calculated backward $m_{wi} = m_{wf} + \sum_{j=i+1}^{n} m_{wj} n \omega_i \theta$, and then the gravity moisture content at each level of suction could be inferred $w_i = m_{wi}/m_s$. Based on the conversion relationship between the volumetric moisture content and the gravity moisture content, we obtained equation $\theta_i = \omega_i \rho_d / \rho_w$, in which the parameters have the following corresponding meaning: m_{wf} is the weight of the water corresponding to the level of maximum suction; m_{wi} is the weight of the water content at each stage of suction; n is the loading level; ω_i is the moisture content of the weight at each level of suction; θ is the volumetric moisture content corresponding to each level of suction; ρ_d is the dry density of the sample; and ρ_w is the density of water at 4°C. By repeating the above test process, the SWCC of remolded loess with different void ratios was obtained.

4.2. Model Verification

4.2.1. Calibration of Model Parameters. The test results of the SWCC of remolded loess with different void ratios were used to verify the reliability of the new model. To calculate the SWCC at different void ratios, a certain void ratio was used as the initial void ratio to calibrate the parameters. This paper adopts an initial void ratio of $e_0 = 0.85$ for model parameter calibration. After the parameters were obtained, the new model could be applied to predict the hydraulic characteristic of loess with different pores. Based on equation (6), we obtained the effective saturation based on the V-G model and combined it with the definition of effective saturation:

$$\theta = \theta_r + (\theta_s - \theta_r)\left(1 + \left(\alpha \frac{(e_0/(1+e_0))^{1/b}\left[1 - (e_i/(1+e_i))^{1/b}\right]}{\left[1 - (e_0/(1+e_0))^{1/b}\right](e_i/(1+e_i))^{1/b}} s\right)^n\right)^{-m}, \tag{46}$$

where $e_i = e_0 = 0.85$, $\xi_{1i} = 1$, and the above equation regresses into the V-G model. The model parameters were calibrated according to the test value of the SWCC test at a void ratio of 0.85. Judging from the above equation, when considering the void ratio, the SWCC model contains seven parameters, namely, θ_s, θ_r, m, n, α, e_0, and b. Of these, $m = 1 - 1/n$. The model can be simplified into 6 parameters. Parameters θ_s, θ_r, n, and α are calibrated as follows: θ_s can be obtained by converting the saturation level of the saturated soil in the initial state; θ_r is determined by the volumetric moisture content in the unsaturated, remaining state proposed by Mualem; and soil parameters n and α can be determined by fitting the test curve. In addition, e_0 is a certain initial void ratio that has the value of 0.85 in this paper, and b is calibrated by the relationship between the pore and the average pore radius. For different void ratios, b varies. Through fitting, the following pairs are gained: when the void ratio is 0.8, $b = 0.15$; when the void ratio is 0.75, $b = 0.2$; when the void ratio is 0.7, $b = 0.25$; when the void ratio is 0.65, $b = 0.3$; and when the void ratio is 0.6, $b = 0.35$. The calibration curve of the model parameters can be seen in Figure 7, and the final model parameters are shown in Table 2.

4.2.2. Prediction of SWCC Model. Under the condition that the calibrated model parameters are obtained, the SWCC of

(a) (b)

Figure 6: Preparation of remolded loess sample.

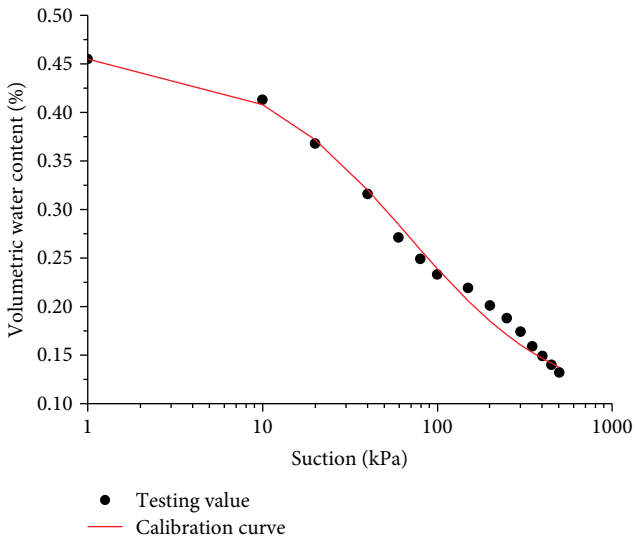

Figure 7: Calibration curve of the model.

Table 2: Calibration of model parameters.

Item	θ_s	θ_r	n	α
Parameter values	0.455	0.095	2.0	0.015

loess that at any void ratio can be predicted according to equation (46). Figures 8–12 show the comparison between the model prediction results and the test results for different void ratios. We can see that the closer the void ratio is to 0.85, the more accurate the prediction results are; the farther it is from 0.85, the more the prediction results of the model in the initial suction section gradually deviate from the test results. When the suction is greater than 100 kPa, the prediction results are still in good agreement with the test results, indicating that the model proposed by this paper can be used to predict the SWCC of unsaturated loess considering pore deformation. Meanwhile, when the void ratio is far from the reference calibration, the model prediction results will gradually show some deviation. The model parameters are obtained by calibration with the reference void ratio. Therefore, the closer the void ratio is to the reference void ratio, the more accurate the model prediction results are. Although the SWCC model considering pore deformation can predict overall changes in soil-water characteristics of the soil at different void ratios, the model is based on the V-G model and therefore inherits some of its inherent shortcomings. The imitative effect of the curve section before the air suction at the low-suction section is not significant. This is especially the case when the difference from the basic calibration void ratio is significant. The more obvious errors in the predictions occur in the low-suction section. When applying this model, we choose the intermediate void ratio to calibrate the model parameters, and we then obtained predictions of the SWCC under different pore conditions on both sides. In addition, if a considerable amount of the soil-water test data of the unsaturated loess was accumulated later, the average value of all data calibration parameters were considered the model parameter values, which we used to predict the soil-water characteristic changes of similar soils under different pore deformation conditions.

4.3. Discussion of Model Parameters. The pore deformation has an obvious influence on the SWCC of the unsaturated loess. After introducing the void ratio parameter, we found that the model prediction results were closely related to parameters e, n, and α. In the next section of this paper, we will discuss the effects of different e, n, and α values on the model results. When analyzing the influence of e, we assumed that n equals 2 and α equals 0.015. When analyzing the influence of n, we assumed that e_0 is 0.85, e_i is 0.8, and α is 0.015. When analyzing the influence of α, we assumed that e_0 is 0.85, e_i is 0.8, and n takes 2.

Figure 13 shows the influence of different values of soil parameter e on the SWCC of unsaturated loess. It can be seen from the figure that the change in the void ratio has an obvious influence on the change of the SWCC. With the increase of the void ratio, the sensitivity of the suction change and volumetric moisture content increases, which heightens especially when the suction exceeds the suction value of intake air. This indicates that pore deformation induced by factors such as loading and water immersion has obvious influence on the soil-water characteristics of the soil and must be considered in practice. The model in this paper can accurately describe the variation of the SWCC under different pore conditions. In fact, the volumetric moisture content-suction-void ratio can be considered the soil-water characteristic surface in a three-dimensional space. A set of soil-water

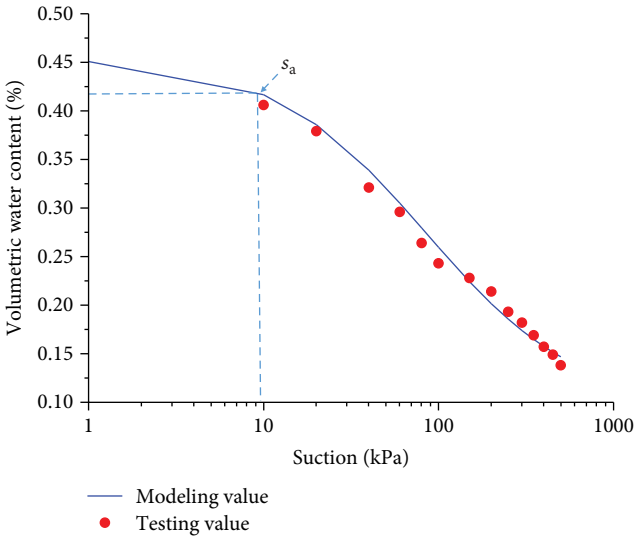

Figure 8: Result comparison at the void ratio of 0.8.

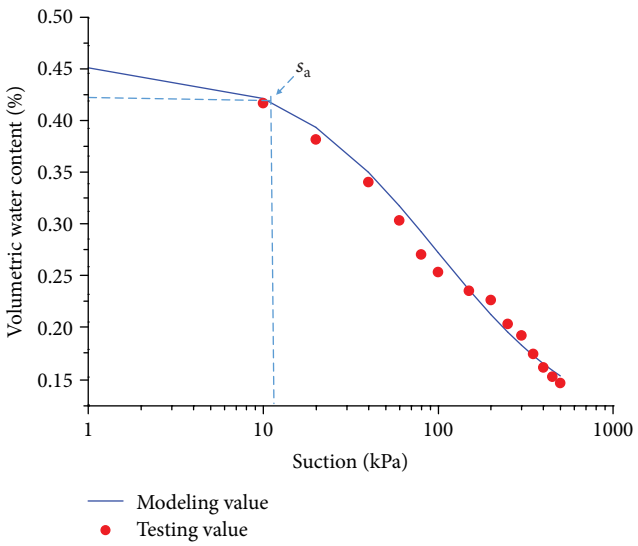

Figure 9: Result comparison at the void ratio of 0.75.

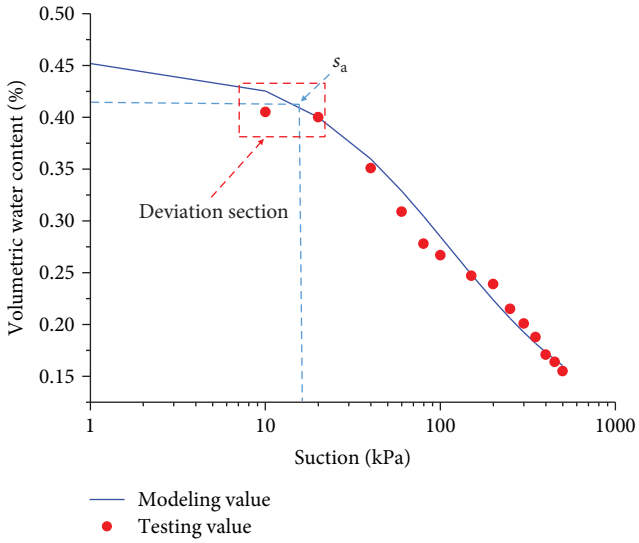

Figure 10: Result comparison at the void ratio of 0.7.

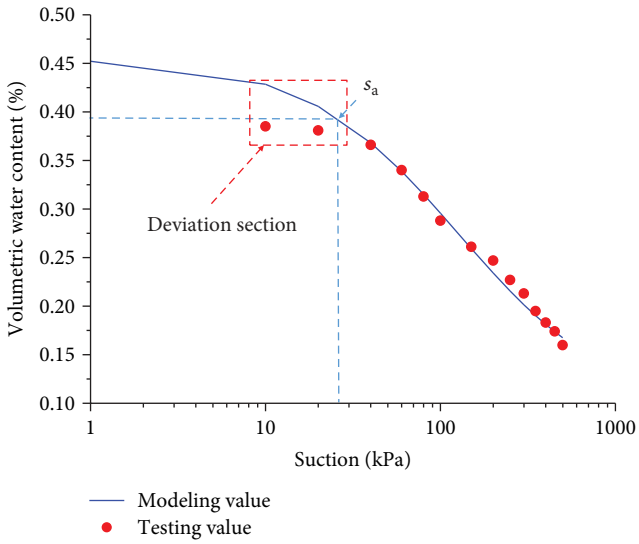

Figure 11: Result comparison at the void ratio of 0.65.

characteristic test parameters can be calibrated based on experience when there is no test data, predicting the evolution law of the SWCC under different pore conditions on the three-dimensional surface. When sufficient test data was accumulated, the average value of the calibrated parameters can be used to predict the variation law of the SWCC under different pore conditions on the three-dimensional curved surface.

Figure 14 shows the influence of different values of soil parameter n on the SWCC. It can be seen from the figure that the SWCC is sensitive to the value of n. When the suction value exceeds 10 kPa, the impact is even more obvious; in the low suction section, the value of n has a relatively weak influence on the curve. As the value of n increases, the suction variation corresponding to changes in water content per unit volume is small, indicating that the relationship between soil suction and water content sensitivity decreases. When n increases to a certain value, its influence on the SWCC gradually weakens with further increases in the n value. Therefore, the value of n reflects the sensitivity of soil moisture content and suction change [7, 24], and it is critical to the accuracy of the model's predictions for the value of n to be reasonably determined through test data.

Figure 15 shows the influence of different values of soil parameter α on the SWCC. It can be seen from the figure that the influence of α on the curve is significant, whether it is in the low-suction section or the high-suction section. When the α value is small, the suction value of the soil intake is relatively large, and the influence of soil immersion and humidification on the curve is relatively small. As the α value increases, the soil suction value decreases, the influence of soil immersion and humidification on the

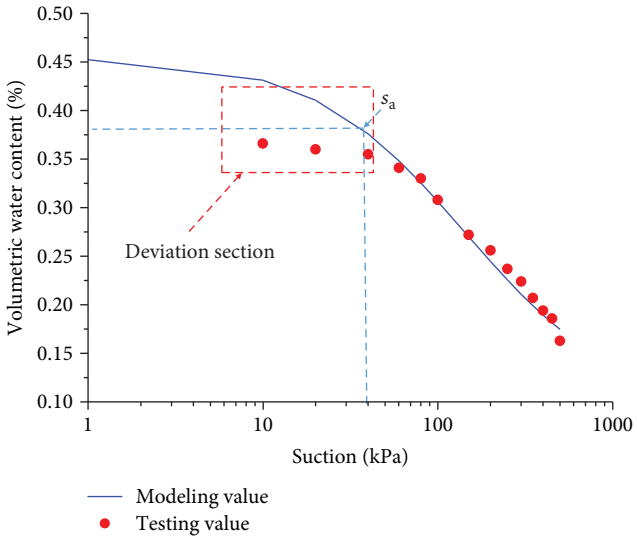

Figure 12: Result comparison at the void ratio of 0.6.

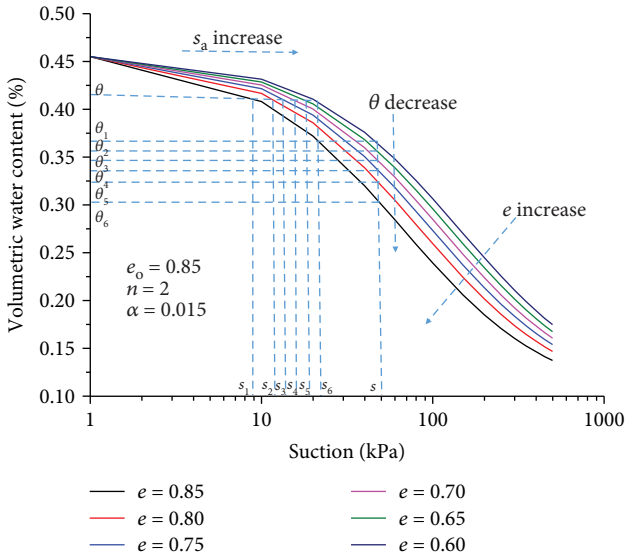

Figure 13: Influence of e on the SWCC.

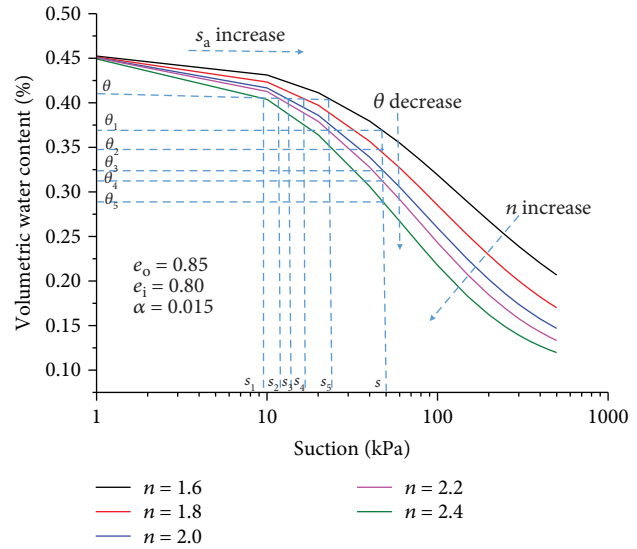

Figure 14: Influence of n on the SWCC.

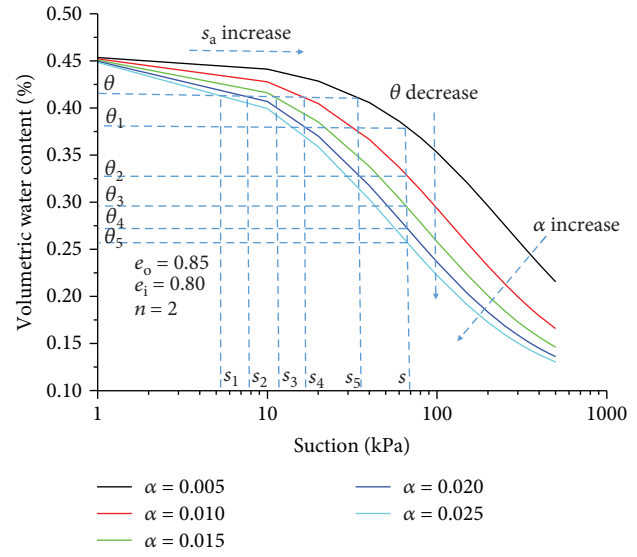

Figure 15: Influence of α on the SWCC.

SWCC becomes increasingly obvious, the suction change corresponding to the change in soil moisture content per unit volume is small, and the relationship between soil suction and moisture content sensitivity decreases. However, when the value of α reaches a certain value, its influence on the SWCC gradually weakens with further increases in the n value.

Figure 16 shows the relationship between the volumetric water content and void ratio when the suction value is the same. As can be seen from the figure, the curve can be divided into sensitivity change section, transition section, and stable section. When the suction is kept constant, the decrease of the void ratio will lead to an increase in volumetric water content. For the same void ratio, the smaller the suction, the larger the volumetric water content. For the same volumetric water content, the larger the suction, the smaller the void ratio. This shows that under the condition of isotropic compression, even if the soil suction remains unchanged, the compaction of the pores in the soil will lead to an increase in saturation.

5. Conclusions

In this paper, we established a new SWCC for predicting the hydraulic characteristics of unsaturated loess with different pore states, and we conducted tests of remolded loess to validate the capability of the new model. The conclusions are as follows:

(1) Based on the assumption of local equilibrium, we defined the expression of the pore density function, discussed the pore distribution of the porous soil medium, and provided the PVF of any WIPD state

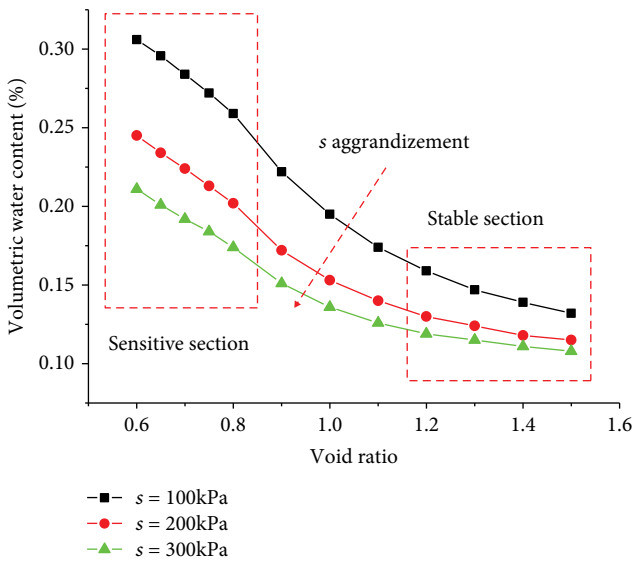

Figure 16: Relation of volumetric water content and void ratio.

(2) By introducing the compression factor and shift factor, we provided a description of the variation law of the pore distribution curve caused by the WIPD of unsaturated loess, and we inferred the relationship between pore indicator e and the compression and shift factors

(3) Based on the PVF, we introduced the pore indicator into the classical V-G model, and we built an SWCC model of unsaturated loess considering the influence of WIPD. The model contains six parameters. When the pore deformation was not considered, the model regressed into a classical V-G model

(4) We carried out the soil-water characteristics tests of unsaturated loess under different pore conditions. The model parameters were calibrated, and the model results were verified under different pore conditions. The results showed that the model has good simulation ability and can accurately predict the evolution of the SWCC of loess under different pore deformation conditions

(5) The impact of parameters of n, e, and α on the model were investigated. The relationship between the volumetric water content and the void ratio at the same suction was discussed in detail, and it was found that the WIPD has the most obvious effect on the SWCC of loess

Data Availability

The data used to support the findings of this study are available from the corresponding authors upon request.

Conflicts of Interest

The authors declare that they have no conflicts of interest.

Acknowledgments

This research was financially supported by grants of the National Science Foundation of China (51378004 and 51578447), Postdoctoral Science Foundation of China (2018M643809XB), and Talent Foundation of Xi'an University of Architecture and Technology (RC1803).

References

[1] J. Lai, J. Qiu, H. Fan, Q. Zhang, J. Wang, and J. Chen, "Fiber bragg grating sensors-based in-situ monitoring and safety assessment of loess tunnel," *Journal of Sensors*, vol. 2016, pp. 1–10, 2016.

[2] G. Tao, Y. Chen, and L. Kong, "A simple fractal-based model for soil-water characteristic curves incorporating effects of initial void ratios," *Bulletin of Engineering Geology and the Environment*, vol. 76, no. 3, pp. 1085–1095, 2018.

[3] Y. Jiang, W. Chen, G. Wang, G. Sun, and F. Zhang, "Influence of initial dry density and water content on the soil–water characteristic curve and suction stress of a reconstituted loess soil," *Bulletin of Engineering Geology and the Environment*, vol. 76, no. 3, pp. 1085–1095, 2017.

[4] J. Qiu, X. Wang, J. Lai, Q. Zhang, and J. Wang, "Response characteristics and preventions for seismic subsidence of loess in Northwest China," *Natural Hazards*, vol. 92, no. 3, pp. 1909–1935, 2018.

[5] Y. Y. Li, S. S. Xu, H. Q. Liu, E. Ma, and L. Wang, "Displacement and stress characteristics of tunnel foundation in collapsible loess ground reinforced by jet grouting columns," vol. 2018, Article ID 2352174, Advances in Civil Engineering, 2018.

[6] Y. Mualem, "A new model for predicting the hydraulic conductivity of unsaturated porous media," *Water Resources Research*, vol. 12, no. 3, pp. 513–522, 1976.

[7] S. Huang, S. L. Barbour, and D. G. Fredlund, "Development and verification of a coefficient of permeability function for a deformable unsaturated soil," *Canadian Geotechnical Journal*, vol. 35, no. 3, pp. 411–425, 1998.

[8] D. Sheng and A. N. Zhou, "Coupling hydraulic with mechanical models for unsaturated soils," *Canadian Geotechnical Journal*, vol. 48, no. 5, pp. 826–840, 2011.

[9] R. H. Brooks and A. T. Corey, *Hydraulic Properties of Porous Media*, Colorado State University, Fort Collins, 1964.

[10] A. R. Russell and O. Buzzi, "A fractal basis for soil-water characteristics curves with hydraulic hysteresis," *Geotechnique*, vol. 62, no. 3, pp. 269–274, 2012.

[11] C. F. Chiu, W. M. Yan, and K. V. Yuen, "Reliability analysis of soil-water characteristics curve and its application to slope stability analysis," *Engineering Geology*, vol. 135-136, no. 5, pp. 83–91, 2012.

[12] A. Azizi, C. Jommi, and G. Musso, "A water retention model accounting for the hysteresis induced by hydraulic and mechanical wetting-drying cycles," *Computers and Geotechnics*, vol. 87, pp. 86–98, 2017.

[13] J. Qiu, Y. Qin, J. Lai et al., "Structural response of the metro tunnel under local dynamic water environment in loess strata," *Geofluids*, vol. 2019, Article ID 8541959, 16 pages, 2019.

[14] J. Qiu, Y. Xie, H. Fan, Z. Wang, and Y. Zhang, "Centrifuge modelling of twin-tunnelling induced ground movements in loess strata," *Arabian Journal of Geosciences*, vol. 10, no. 22, p. 493, 2017.

[15] J. X. Lai, S. Y. He, J. L. Qiu et al., "Characteristics of seismic disasters and aseismic measures of tunnels in Wenchuan earthquake," *Environmental Earth Sciences*, vol. 76, no. 2, p. 94, 2017.

[16] J. L. Qiu, X. L. Wang, S. Y. He, H. Liu, J. Lai, and L. Wang, "The catastrophic landside in Maoxian County, Sichuan, SW China, on June 24, 2017," *Natural Hazards*, vol. 89, no. 3, pp. 1485–1493, 2017.

[17] J. B. Wang, Z. P. Song, B. Y. Zhao, X. Liu, J. Liu, and J. Lai, "A study on the mechanical behavior and statistical damage constitutive model of sandstone," *Arabian Journal for Science and Engineering*, vol. 43, no. 10, pp. 5179–5192, 2018.

[18] B. T. Lai, A. Fabbri, H. Wong, and D. Branque, "Poroelastic behaviour of fine compacted soils in the unsaturated to saturated transition zone," *Computers and Geotechnics*, vol. 69, no. 9, pp. 627–640, 2015.

[19] J. Li, Z. Y. Yin, Y. Cui, and P. Y. Hicher, "Work input analysis for soils with double porosity and application to the hydromechanical modeling of unsaturated expansive clays," *Canadian Geotechnical Journal*, vol. 54, no. 2, pp. 173–187, 2017.

[20] P. Li, S. Vanapalli, and T. Li, "Review of collapse triggering mechanism of collapsible soils due to wetting," *Journal of Rock Mechanics and Geotechnical Engineering*, vol. 8, no. 2, pp. 256–274, 2016.

[21] N. Lu and M. Khorshidi, "Mechanisms for soil-water retention and hysteresis at high suction range," *Journal of Geotechnical and Geoenvironmental Engineering*, vol. 141, no. 8, article 04015032, 2015.

[22] Z. Hu, K. Du, J. Lai, and Y. Xie, "Statistical Analysis of Influence of Cover Depth on Loess Tunnel Deformation in NW China," *Advances in Civil Engineeringl*, vol. 2019, pp. 1–12, 2019.

[23] Y. Tang, H. A. Taiebat, and A. R. Russell, "Numerical modeling of consolidation of unsaturated soils considering hydraulic hysteresis," *International Journal of Geomechanics*, vol. 18, no. 2, article 04017136, 2018.

[24] A. Zhou, S. Wu, J. Li, and D. Sheng, "Including degree of capillary saturation into constitutive modelling of unsaturated soils," *Computers and Geotechnics*, vol. 95, pp. 82–98, 2018.

[25] D. Sheng, D. G. Fredlund, and A. Gens, "A new modelling approach for unsaturated soils using independent stress variables," *Canadian Geotechnical Journal*, vol. 45, no. 4, pp. 511–534, 2008.

[26] A. Zhou and D. Sheng, "An advanced hydro-mechanical constitutive model for unsaturated soils with different initial densities," *Computers and Geotechnics*, vol. 63, pp. 46–66, 2015.

[27] E. Gholizadeh and M. Latifi, "A coupled hydro-mechanical constitutive model for unsaturated frictional and cohesive soil," *Computers and Geotechnics*, vol. 98, pp. 69–81, 2018.

[28] A. Gens, "Soil-environment interactions in geotechnical engineering," *Geotechnique*, vol. 60, no. 1, pp. 3–74, 2010.

[29] E. C. Leong and H. Rahardjo, "Review of soil-water characteristic curve equations," *Journal of Geotechnical and Geoenvironmental Engineering*, vol. 123, no. 12, pp. 1106–1117, 1997.

[30] G. F. N. Gitirana Jr and D. G. Fredlund, "Soil-water characteristic curve equation with independent properties," *Journal of Geotechnical and Geoenvironmental Engineering*, vol. 130, no. 2, pp. 209–212, 2004.

[31] D. Gallipoli, "A hysteretic soil-water retention model accounting for cyclic variations of suction and void ratio," *Geotechnique*, vol. 62, no. 7, pp. 605–616, 2012.

[32] C. A. Burger and C. D. Shackelford, "Evaluating dual porosity of pelletized diatomaceous earth using bimodal soil–water characteristic curve functions," *Canadian Geotechnical Journal*, vol. 38, no. 1, pp. 53–66, 2001.

[33] D. G. Fredlund and A. Xing, "Equations for the soil-water characteristic curve," *Canadian Geotechnical Journal*, vol. 31, no. 4, pp. 521–532, 1994.

[34] N. Lu and W. J. Likos, "Suction stress characteristic curve for unsaturated soil," *Journal of Geotechnical and Geoenvironmental Engineering*, vol. 132, no. 2, pp. 131–142, 2006.

[35] N. Lu, "Generalized soil water retention equation for adsorption and capillarity," *Journal of Geotechnical and Geoenvironmental Engineering*, vol. 142, no. 10, article 04016051, 2016.

[36] N. Lu, J. W. Godt, and D. T. Wu, "A closed-form equation for effective stress in unsaturated soil," *Water Resources Research*, vol. 46, no. 5, article W05515, 2010.

[37] D. Sheng, "Review of fundamental principles in modelling unsaturated soil behaviour," *Computers and Geotechnics*, vol. 38, no. 6, pp. 757–776, 2011.

[38] C. W. W. Ng, J. Xu, and S. Y. Yung, "Effects of wetting–drying and stress ratio on anisotropic stiffness of an unsaturated soil at very small strains," *Canadian Geotechnical Journal*, vol. 46, no. 9, pp. 1062–1076, 2009.

[39] L. Kong, H. M. Sayem, and H. Tian, "Influence of drying-wetting cycles on soil-water characteristic curve of undisturbed granite residual soils and microstructure mechanism by nuclear magnetic resonance (NMR) spin-spin relaxation time (T-2) relaxometry," *Canadian Geotechnical Journal*, vol. 55, no. 2, pp. 208–216, 2018.

[40] W. L. Xie, P. Li, S. K. Vanapalli, and J. D. Wang, "Prediction of the wetting-induced collapse behaviour using the soil-water characteristic curve," *Journal of Asian Earth Sciences*, vol. 151, pp. 259–268, 2018.

[41] S. K. Vanapalli, D. G. Fredlund, and D. E. Pufahl, "The influence of soil structure and stress history on the soil–water characteristics of a compacted till," *Geotechnique*, vol. 49, no. 2, pp. 143–159, 1999.

[42] S. K. Vanapalli, D. G. Fredlund, D. E. Pufahl, and A. W. Clifton, "Model for the prediction of shear strength with respect to soil suction," *Canadian Geotechnical Journal*, vol. 33, no. 3, pp. 379–392, 1996.

[43] A. N. Zhou, "A contact angle-dependent hysteresis model for soil–water retention behaviour," *Computers and Geotechnics*, vol. 49, pp. 36–42, 2013.

[44] J. Lai, K. Wang, J. Qiu, F. Niu, J. Wang, and J. Chen, "Vibration response characteristics of the cross tunnel structure," *Shock and Vibration*, vol. 2016, pp. 1–16, 2016.

[45] Z. J. Zhou, C. N. Ren, G. J. Xu, H. C. Zhan, and T. Liu, "Dynamic failure mode and dynamic response of high slope using shaking table test," *Shock and Vibration*, vol. 2019, Article ID 4802740, 19 pages, 2019.

[46] P. Delage, M. Audiguier, Y. J. Cui, and M. D. Howat, "Microstructure of a compacted silt," *Canadian Geotechnical Journal*, vol. 33, no. 1, pp. 150–158, 1996.

[47] G. Della Vecchia, A. C. Dieudonné, C. Jommi, and R. Charlier, "Accounting for evolving pore size distribution in water retention models for compacted clays," *International Journal for Numerical and Analytical Methods in Geomechanics*, vol. 39, no. 7, pp. 702–723, 2015.

[48] D. Gallipoli, S. J. Wheeler, and M. Karstunen, "Modelling the variation of degree of saturation in a deformable

unsaturated soil," *Geotechnique*, vol. 53, no. 1, pp. 105–112, 2003.

[49] R. Hu, Y.-F. Chen, H.-H. Liu, and C.-B. Zhou, "A water retention curve and unsaturated hydraulic conductivity model for deformable soils: consideration of the change in pore-size distribution," *Geotechnique*, vol. 63, no. 16, pp. 1389–1405, 2013.

[50] X. Li, J. H. Li, and L. M. Zhang, "Predicting bimodal soil-water characteristic curves and permeability functions using physically based parameters," *Computers and Geotechnics*, vol. 57, pp. 85–96, 2014.

[51] X.L. Luo, D.Y. Li, Y. Yang, and S.R. Zhang, "Spatiotemporal Traffic Flow Prediction with KNN and LSTM," *Journal of Advanced Transportation*, vol. 2019, pp. 1–10, 2019.

[52] R. Monroy, L. Zdravkovic, and A. Ridley, "Evolution of microstructure in compacted London clay during wetting and loading," *Geotechnique*, vol. 60, no. 2, pp. 105–119, 2010.

[53] J. Wang, Q. Huo, Z. Song, and Y. Zhang, "Study on adaptability of primary support arch cover method for large-span embedded tunnels in the upper-soft lower-hard stratum," *Advances in Mechanical Engineering*, vol. 11, no. 1, pp. 1–15, 2019.

[54] M. Wijaya and E. C. Leong, "Equation for unimodal and bimodal soil–water characteristic curves," *Soils and Foundations*, vol. 56, no. 2, pp. 291–300, 2016.

[55] A. Revil and N. Lu, "Unified water isotherms for clayey porous materials," *Water Resources Research*, vol. 49, no. 9, pp. 5685–5699, 2013.

[56] A. Satyanaga, H. Rahardjo, E. C. Leong, and J. Y. Wang, "Water characteristic curve of soil with bimodal grain-size distribution," *Computers and Geotechnics*, vol. 48, no. 5, pp. 51–61, 2013.

[57] D. A. Sun, H. Matsuoka, and Y. F. Xu, "Collapse behavior of compacted clays in suction-controlled triaxial tests," *Geotechnical Testing Journal*, vol. 27, no. 4, pp. 11418-11419, 2004.

[58] D. Sun, D. Sheng, and Y. Xu, "Collapse behaviour of unsaturated compacted soil with different initial densities," *Canadian Geotechnical Journal*, vol. 44, no. 6, pp. 673–686, 2007.

[59] H. Rahardjo, X. F. Nong, D. T. T. Lee, E. C. Leong, and Y. K. Fong, "Expedited soil-water characteristic curve tests using combined centrifuge and chilled mirror techniques," *Geotechnical Testing Journal*, vol. 41, no. 1, pp. 207–217, 2018.

[60] P. H. Simms and E. K. Yanful, "Measurement and estimation of pore shrinkage and pore distribution in a clayey till during soil-water characteristic curve tests," *Canadian Geotechnical Journal*, vol. 38, no. 4, pp. 741–754, 2001.

[61] L. Zhang and Q. Chen, "Predicting bimodal soil-water characteristic curves," *Journal of Geotechnical and Geoenvironmental Engineering*, vol. 131, no. 5, pp. 666–670, 2005.

[62] M. Nuth and L. Laloui, "Advances in modelling hysteretic water retention curve in deformable soils," *Computers and Geotechnics*, vol. 35, no. 6, pp. 835–844, 2008.

[63] N. Mahabadi, S. Dai, Y. Seol, T. Sup Yun, and J. Jang, "The water retention curve and relative permeability for gas production from hydrate-bearing sediments: pore-network model simulation," *Geochemistry, Geophysics, Geosystems*, vol. 17, no. 8, pp. 3099–3110, 2016.

[64] N. Mahabadi, X. Zheng, and J. Jang, "The effect of hydrate saturation on water retention curves in hydrate-bearing sediments," *Geophysical Research Letters*, vol. 43, no. 9, pp. 4279–4287, 2016.

[65] H. Tanaka, D. R. Shiwakoti, N. Omukai, F. Rito, J. Locat, and M. Tanaka, "Pore size distribution of clayey soils measured by mercury intrusion porosimetry and its relation to hydraulic conductivity," *Soils and Foundations*, vol. 43, no. 6, pp. 63–73, 2003.

[66] M. T. Van Genuchten, "A closed-form equation for predicting the hydraulic conductivity of unsaturated soils," *Soil Science Society of America Journal*, vol. 44, no. 5, pp. 892–898, 1980.